Manuscript submitted to
AIMS' Journals
Volume **X**, Number **0X**, XX **200X**

doi:10.3934/xx.xx.xx.xx

pp. **X–XX**

DYNAMICAL STABILIZATION AND TRAVELING WAVES IN INTEGRODIFFERENCE EQUATIONS

Adèle Bourgeois, Victor LeBlanc

Department of Mathematics and Statistics
University of Ottawa
Ottawa, ON K1N 6N5, CANADA

and Frithjof Lutscher*

Department of Mathematics and Statistics
Department of Biology
University of Ottawa
Ottawa, ON K1N 6N5, CANADA

(Communicated by the associate editor name)

Abstract. Integrodifference equations are discrete-time analogues of reaction-diffusion equations and can be used to model the spatial spread and invasion of non-native species. They support solutions in the form of traveling waves, and the speed of these waves gives important insights about the speed of biological invasions. Typically, a traveling wave leaves in its wake a stable state of the system. Dynamical stabilization is the phenomenon that an unstable state arises in the wake of such a wave and appears stable for potentially long periods of time, before it is replaced with a stable state via another transition wave. While dynamical stabilization has been studied in systems of reaction-diffusion equations, we here present the first such study for integrodifference equations. We use linear stability analysis of traveling-wave profiles to determine necessary conditions for the emergence of dynamical stabilization and relate it to the theory of stacked fronts. We find that the phenomenon is the norm rather than the exception when the non-spatial dynamics exhibit a stable two-cycle.

1. **Introduction.** *Dynamical stabilization* is a concept that was first described by [22] in the context of a predator-prey reaction-diffusion model. It describes the observation that a locally unstable state of a non-spatial model may appear stable (over long times) in a corresponding spatial reaction-diffusion model (see below for details). Integrodifference equations (IDEs) describe local reaction and spatial spread in discrete time and share many close connections with reaction-diffusion equations, yet the phenomenon of dynamical stabilization has not been formally

2010 *Mathematics Subject Classification.* Primary: 37L15, 92D25; Secondary: 37N25.

Key words and phrases. Stacked wave fronts, integro-difference equations, stability, invasion speeds.

VL and FL are supported by respective Discovery Grants from the Natural Sciences and Engineering Research Council (NSERC) of Canada (RGPIN-2016-04318 and RGPIN-2016-04795). FL is grateful for a Discovery Accelerator Supplement award from NSERC (RGPAS 492878-2016). FL thanks the participants of the workshop "Integrodifference equations in spatial ecology: 30 years and counting" (16w5121) at the Banff International Research Station for their feedback on an oral presentation of this material.

* Corresponding author: flutsche@uottawa.ca.

studied in IDEs. In our recent work, we observed dynamical stabilization numerically, but did not study it formally. Here, we present a more formal investigation of this phenomenon, based on stability analysis and bifurcation theory.

A non-spatial predator-prey model in continuous time may have a positive, unstable coexistence state surrounded by an asymptotically stable limit cycle [5]. When adding random movement of each species in one-dimensional space (via diffusion), one typically observes the following qualitative behavior when both species are introduced locally, say in the same interval. First, the prey species spreads spatially at a relatively fast rate, then, somewhat slower, the predator species spreads into the region where the prey is now established [7, 8, 27, 28]. When the coexistence state is unstable, one may observe a region that spreads even more slowly, where the two species oscillate locally. (For example, see Figure 2 in [22].) In the region where both species are present but not (yet) oscillating, their respective densities are close to the steady-state densities of the non-spatial model. The length of this region can grow over time, so that a plateau forms where the populations appear to be stable, even though the corresponding steady state in the non-spatial model is unstable. This spatial phenomenon was termed 'dynamical stabilization'. In the words of the authors [22]: "a locally unstable equilibrium of the system can be made dynamically stable in the full diffusion-reaction system".

The ecological implications of such dynamics are obvious. A predator-prey community that has been stable for a long time may seemingly suddenly begin to oscillate without any apparent reason. Empirical research might be conducted as to the biotic or abiotic reasons of this destabilization. Yet, no environmental change need to have occurred. It might simply be the case that temporary dynamical stabilization is replaced by asymptotic oscillations.

The spatial region where dynamical stabilization takes place is bounded by two moving objects: the spatial advance of the predator ahead of the region and the spatial advance of the oscillations behind. The authors in [22] concluded that a necessary condition for dynamical stabilization to occur is that the first of these objects move faster than the second.

Even though the phenomenon of dynamical stabilization is difficult to study in reaction-diffusion equations (since it requires at least two coupled equations) much progress has been made in recent years, see e.g. [4, 34] and references therein. A scalar reaction-diffusion equation, however, has monotone solution dynamics, and can therefore never support these complex patterns.

Integrodifference equations (IDEs) are used to model the dynamics of a biological population with discrete, non-overlapping generations and temporally separated growth and dispersal phases [18]. They are particularly well-suited to represent the life cycle of many plant and insect species [17], and have been applied to many biological invasions [3, 10]. An IDE projects the population density $N_t(x)$ at any point x in space from generation t to generation $t+1$ according to the two processes of growth and dispersal. The growth phase, during which individuals are spatially stationary, is modelled by a *growth function* F. The dispersal phase, during which no population dynamics occur, is described by a *dispersal kernel* K. The dispersal kernel represents the probability density function of individual (signed) dispersal distances [26]. The *next generation operator* Q that maps the density at time t to the density at time $t+1$ is given by the composition of growth and dispersal as the

convolution integral operator

$$N_{t+1}(x) = Q[N_t](x) = [K * F(N_t)](x) = \int_{\mathbb{R}} K(x-y)F(N_t(y))dy. \tag{1}$$

If growth function F is not monotone (see examples below), then the dynamics of 1 need not be monotone. We shall show here that in this case, one can observe the phenomenon of dynamical stabilization in the scalar IDE.

The qualitative dynamics of operator Q depend on the properties of the growth function and the dispersal kernel. Here, we focus on the (scaled) Ricker function

$$F(N) = N\exp(r(1-N)), \qquad r > 0, \tag{2}$$

and the (scaled) logistic function

$$F(N) = (1+r)N - rN^2, \qquad r > 0. \tag{3}$$

To describe dispersal, we shall always use the Laplace kernel

$$K(x) = \frac{a}{2}e^{-a|x|}, \qquad a > 0, \tag{4}$$

with variance $\sigma^2 = \frac{2}{a^2}$. This kernel can be derived from a continuous random-walk model for individual movement and a Poisson process for stopping the walk [26]. It can also be fit reasonably well to many published data sets [19]. We discuss other choices at the end of our work.

The non-spatial, one-dimensional map $N \mapsto F(N)$ with F as in 2 or 3 has two fixed points, namely $N^* = 0$ and $N^* = 1$. The former is unstable. If $0 < r < 1$, then F is monotone between 0 and 1, and consequently, $N^* = 1$ is globally stable. For $1 < r < 2$, function F has a global maximum between 0 and 1, and its slope at 1 is negative. Nonetheless, the positive fixed point is still stable in this range. At $r = 2$, we have $F'(1) = -1$. A flip bifurcation occurs, in which $N^* = 1$ becomes unstable and a globally stable two-cycle emerges. We denote the values of the two-cycle as $n_\pm$. They satisfy the relations $n_+ = F(n_-) = F(F(n_+))$ and $0 < n_- < 1 < n_+$. This two-cycle is stable when $2 < r < 2.526$ for the Ricker function and $2 < r < 2.449$ for the logistic function but loses stability for larger values of r, when a cascade of period-doubling bifurcations leads to higher-order cycles and chaos. We will not consider the dynamics beyond this point, but refer the reader to standard works for discrete dynamics, e.g. [25] and references therein. Table 1 gives a summary of the behavior of the non-spatial models that is relevant in our work.

Dynamic behavior	Ricker function 2	Logistic function 3
$N^* = 1$ g.a.s. monotone approach	$0 < r < 1$	$0 < r < 1$
$N^* = 1$ g.a.s. oscillatory approach	$1 < r < 2$	$1 < r < 2$
$N^* = 1$ unstable	$2 < r < 2.526$	$2 < r < 2.449$
Stable 2-cycle $n_\pm$		

TABLE 1. Dynamic behavior of the map $N \mapsto F(N)$ with F as in 2 or 3. The abbreviation 'g.a.s.' stands for globally asymptotically stable within all non-stationary, non-negative solutions.

Many aspects of the spatial spread dynamics of IDE 1 have been studied in great detail. One important concept is that of the "asymptotic spreading speed"

[35]. This quantity, typically denoted by c^*, gives the speed at which a locally introduced population will eventually spread in space. It has long been known that IDE 1 has an asymptotic spreading speed if F is monotone increasing and concave down between 0 and 1; see [36] for a precise statement of this result. The following explicit formula holds in this case [36, 37]

$$c^* = \inf_{s>0} \frac{1}{s} \ln \left(F'(0) \int K(x) e^{sx} dx \right). \tag{5}$$

Furthermore, for all $c \geq c^*$, there exists a family of monotone traveling waves, i.e., solutions of the form $N_t(x) = \widetilde{N}(x + ct)$. This theory applies to our model when F is the Ricker or logistic function and $0 < r < 1$.

More recently, it was shown that the spreading speed also exists when F has an intermediate maximum, provided that the steady state at $N^* = 1$ is stable [13, 20, 38]. Also, there exists a not necessarily monotone traveling wave solution for all $c \geq c^*$. Under some additional conditions [13, 21, 39], these traveling waves connect the unstable state $N^* = 0$ to the stable state $N^* = 1$. This result applies when F is the Ricker or logistic function for $1 < r < 2$.

What happens when the positive state is unstable, is less clear. The spreading speed still exists [20], but different simulations of the spatial profile of the spreading population show different phenomena [16, 20]. In our own recent work [1, 2], we considered the case that the non-spatial model $N \mapsto F(N)$ has a stable two-cycle and studied the corresponding spatial model via the second-iterate operator $Q \circ Q$. We proved the existence of a *generalized spreading speed*, the speed at which a local addition to the unstable state $N^* = 1$ will eventually spread in space. We also showed the existence of monotone and non-monotone traveling waves that connect the state $N^* = 1$ with the states $n_\pm$ of the second-iterate operator. In numerical simulations, we observed *stacked waves*: a traveling profile that connects the unstable state at 0 with the unstable state at 1, followed by a second profile that connects the unstable state at 1 with the stable state at n_+ (or n_-). The first profile travels faster than the second, so that a plateau emerges at the unstable state at 1 and grows in length. This is, of course, another example of dynamical stabilization. Such a stacked wave for the second-iterate operator manifests as dynamical stabilization for the operator Q. A locally introduced population will spread in space and initially seem to settle at the (unstable) state at 1 before the two-cycle oscillations between n_+ and n_- spread spatially and destabilize the plateau. We illustrate this scenario with the Ricker and logistic growth functions in Figure 1.

Remark 1. To create the figures, we performed simulations in MATLAB®, using two independent numerical schemes to evaluate the convolution integral: (i) trapezoidal function `trapz`, and (ii) the Fast-Fourier-Transform (`fft`). Code for the latter was developed by Prof. J. Powell and is available at

(`http://math.usu.edu/powell/wauclass/labs.html`). We performed the simulations on an interval of length 160 with 2^{17} equidistant nodes (for `fft`) and 2^{12} nodes (for `trapz`).

In our previous work [2], we focused on generalized spreading speeds and found the phenomenon of dynamical stabilization numerically, but did not study in detail. Here, we use the complementary approach of traveling wave analysis to study these observations in more detail. In the next section, we introduce our set-up by reducing the integral equation that defines that traveling wave to a second-order delay

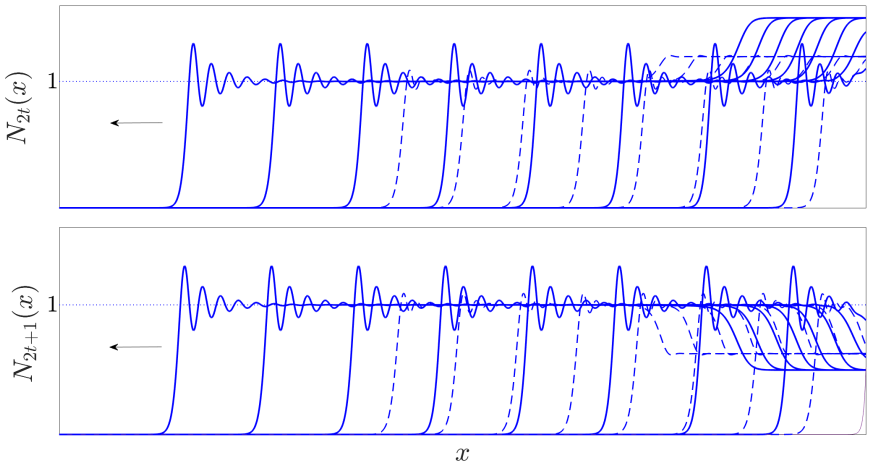

FIGURE 1. Numerical solution of the IDE in 1, plotted for even (top panel) and odd (bottom panel) generations every 10 time steps. The solid lines correspond to the Ricker growth function 2 with $r = 2.2$ and the dashed line to the logistic growth function 3 with $r = 2.44$. The dispersal kernel is the Laplace kernel 4 with $a = 15$. The initial condition was the function $N_0(x) = n_-\chi_{x\leq 10}$.

differential equation. We then study the stability behavior of the steady states of the delay system. The results inform us about the possibility of heteroclinic orbits between these states as well as their qualitative behavior near the states. In Section 3, we summarize the stability results and conclude in which scenarios dynamical stabilization may occur. We illustrate our results by numerical simulations. We end with a discussion that relates our results to the theory of stacked waves and traveling wave-trains.

2. **Traveling-wave analysis.** A traveling-wave profile with speed c is defined by the equation $\widetilde{N}(\cdot + c) = Q[\widetilde{N}](\cdot)$. It is a particular property of the Laplace kernel 4 that the integral equation

$$N(x + c) = \int K(x - y)G(N(y))dy, \tag{6}$$

is equivalent to the second-order delay differential equation

$$N''(x + c) = a^2N(x + c) - a^2G(N(x)), \tag{7}$$

provided N and G are sufficiently smooth [16].

It is tempting and even helpful to look at this system in the 'phase plane', but one needs to keep in mind that the system has a delay and is therefore infinite-dimensional, so that the 'phase plane' does not show the complete picture. In particular, solutions of the delay equation may cross in the 'phase plane.'

By letting $y = x + c$ and $n(y) = N'(y)$, we obtain the system of first-order equations:

$$\begin{aligned} N'(y) &= n(y), \\ n'(y) &= a^2N(y) - a^2G(N(y - c)). \end{aligned} \tag{8}$$

The equilibrium points of this system are given by $(N^*, 0)$, where N^* denotes a fixed point of G. A traveling-wave solution of the IDE with asymptotic densities N_i^* corresponds to a heteroclinic connection between two steady states $(N_i^*, 0)$ in the 'phase plane' of 8. Necessarily, N_i^* are fixed points of G. Therefore, we are interested in studying the stability of the equilibrium points of 8.

More specifically, to justify the existence of the plateau at $N^* = 1$ in the solution of the IDE we need to have two connections in the 'phase plane'. First, there has to be a connection from 0 to 1 for the operator Q. Hence, we set $G = F$ and require that $(0, 0)$ has at least a one-dimensional unstable manifold with non-oscillatory solutions and that $(1, 0)$ has at least a one-dimensional stable manifold. Secondly, there has to be a connection between 1 and some other state for the operator $Q \circ Q$. Hence, we set $G = Q$ and require that $(1, 0)$ has at least a one-dimensional unstable manifold. We shall study the eigenvalues of 8 to determine when these necessary conditions are satisfied. The stability analysis of the point $(0, 0)$ was already done in [16]. We shall review it briefly in the next section.

2.1. **Existence of an Unstable Direction at** $(0, 0)$**.** To determine conditions for the existence of an unstable manifold at $(0, 0)$ we set $G = F$ in 6. The delay differential equations for a wave profile N with speed c are

$$\begin{aligned} N'(y) &= n(y), \\ n'(y) &= a^2 N(y) - a^2 F(N(y - c)), \end{aligned} \tag{9}$$

with equilibria $(0, 0)$ and $(1, 0)$. We linearize this system at $(N^*, 0)$ by letting $N(y) = N^* + M(y)$ to obtain the linear homogeneous system

$$\begin{bmatrix} M'(y) \\ n'(y) \end{bmatrix} = \begin{bmatrix} 0 & 1 \\ a^2 & 0 \end{bmatrix} \begin{bmatrix} M(y) \\ n(y) \end{bmatrix} + \begin{bmatrix} 0 & 0 \\ -a^2 F'(N^*) & 0 \end{bmatrix} \begin{bmatrix} M(y - c) \\ n(y - c) \end{bmatrix}. \tag{10}$$

The characteristic equation of this system is given by [6]

$$\det \begin{bmatrix} -\lambda & 1 \\ a^2(1 - e^{-c\lambda} F'(N^*)) & -\lambda \end{bmatrix} = 0.$$

After scaling, we obtain the transcendental eigenvalue problem

$$1 - \frac{\lambda^2}{(ac)^2} = F'(N^*) e^{-\lambda}. \tag{11}$$

The expression on the left is a concave-down parabola. At $N^* = 0$, we have $F'(N^*) > 0$ so that the expression on the right is a decreasing exponential in λ.

With this set-up, we can briefly summarize the result about $(0, 0)$ from [16]. Recall that we are interested only in non-oscillatory solutions, so that we require the eigenvalue corresponding to the unstable direction to be real. For $N^* = 0$, we have $F'(0) > 1$. Hence, the exponential in 11 is above the quadratic at zero. Therefore, 11 will not have solutions for $\lambda < 0$. For $\lambda > 0$, there can be up to two positive real roots. For a single root, we also have the tangency condition

$$\frac{2\lambda}{(ac)^2} = F'(0) e^{-\lambda}. \tag{12}$$

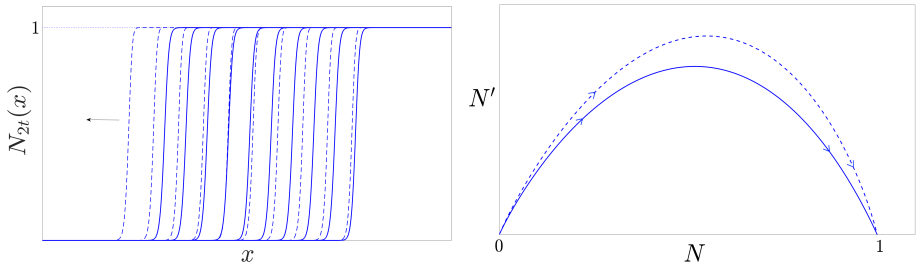

FIGURE 2. Solution of the integrodifference equation (left) and its 'phase plane' (right), where F is the Ricker function with $r = 0.8$ (solid) and $r = 1.03$ (dashed) and K is the Laplace kernel with $a = 15$.

Following the method in [16], we can combine 11 and 12 to obtain a parametric representation for λ as

$$ac = \sqrt{\lambda^2 + 2\lambda}, \qquad F'(0) = \frac{2e^{\lambda}}{2+\lambda}. \tag{13}$$

This representation corresponds specifically to the parametric representation of the asymptotic spreading speed c^* [16]. Thus, we conclude that 11 has one positive real root for $c = c^*$, and two positive real roots for $c > c^*$ since $1 - \frac{\lambda^2}{(ac)^2} > 1 - \frac{\lambda^2}{(ac^*)^2}$. Hence, the necessary condition for a non-oscillating trajectory to move away from $(0,0)$ in the delay differential equation 9 is $c \geq c^*$.

Remark 2. We note that there is an explicit formula of the spreading speed c^* in 5 when K is the Laplace kernel in 4, but this formula does involve the Lambert-W function [2]. The surprising insight from this explicit formula is that the expression ac^* is independent of the parameter a in the Laplace kernel. In particular, the condition in 11 depends on r but is independent of parameter a.

2.2. **Existence of a Stable Direction at** $(1,0)$**.** The set-up for the stability analysis of $(1,0)$ is the same as in the previous section. Here, however, we have $F'(N^*) = F'(1) < 1$. In addition, if $r < 1$, we have $0 < F'(1) < 1$. In this case, the parabola on the left-hand side of 11 lies above the exponential function at zero. Hence, equation 11 will have one positive and one negative real root, independent of c. This result, in combination with the analysis around $(0,0)$, shows that the necessary condition for the existence of a monotone connection between $(0,0)$ and $(1,0)$ is satisfied for $c \geq c^*$. In the 'phase plane', this connection corresponds to the plot shown in Figure 2. Thus, a monotone profile from 0 to 1 in the solution of the integrodifference equation can (and does) exist for $c \geq c^*$.

When F is the Ricker function or the logistic function and $1 < r < 2$, we find that $F'(1) = 1 - r < 0$. In this case, 11 always has a positive real root and may have up to two negative real roots. Analogously to the case above, a unique negative root exists if the tangency condition in 12 with $F'(0)$ replaced by $F'(1)$ is satisfied. When there is a negative real root, we have the necessary condition for the existence of a monotone profile (as explained above). In particular, there can be a monotone traveling-wave profile even if the growth function F is not monotone.

To explore the range of $r > 1$ where we can still expect a monotone profile in the IDE even though the non-spatial map is not monotone, we fix the speed of

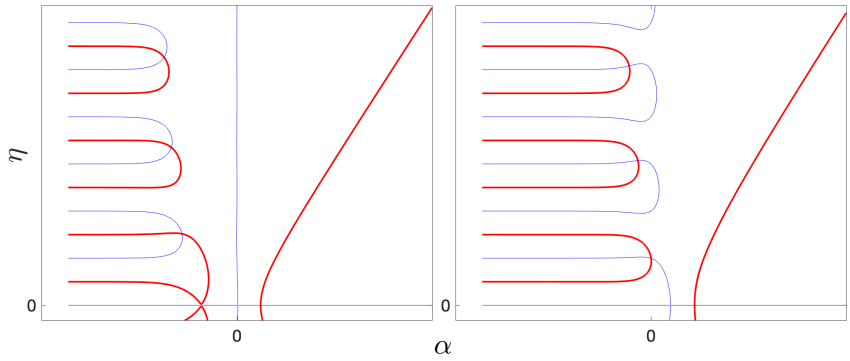

FIGURE 3. Plot of the implicit functions defined by equations 15 (thin blue lines) and 16 (thicker red line) with $c = c^*$ for the Ricker function with $r = 1.0327$ (left) and $r = 2.526$ (right). Note that there are no negative real roots as we chose $r > r^*$. Only the upper half plane is plotted; the lower half plane is symmetric.

the profile to be the smallest possible speed, namely c^*, which depends on r. The intersection and tangency conditions then are

$$1 - \frac{\lambda^2}{(ac^*)^2} = (1-r)e^{-\lambda} \quad \text{and} \quad \frac{2\lambda}{(ac^*)^2} = (1-r)e^{-\lambda}. \tag{14}$$

The left-hand side of the first condition in 14 is increasing in r since c^* is. The right-hand side is decreasing. Hence, there is a unique threshold value $r^* > 1$ below which we can expect monotone traveling waves. Numerically, we find $r^* = 1.0327$ for the Ricker function and $r^* = 1.0686$ for the logistic function. It follows that the IDE 1 has monotone traveling waves of speed $c^*(r)$ for $r < r^*$. As per the previous remark, the condition in 14 depends only on the growth parameter r and is independent of the dispersal parameter a. For an illustration of this case, please see Figure 2.

When no real negative eigenvalues exist, we look for complex eigenvalues with negative real part. If such an eigenvalue exists, we expect that there exists a trajectory in the 'phase-plane' that approaches $(1, 0)$ in an oscillatory manner. This would correspond to a non-monotone traveling wave of the IDE.

We let $\lambda = \alpha + i\eta$ with $\alpha, \eta \in \mathbb{R}$ in 11 and separate real and imaginary parts to obtain the pair of equations

$$1 - \frac{\alpha^2 - \eta^2}{(ac)^2} = (1-r)e^{-\alpha}\cos(\eta), \tag{15}$$

$$\frac{2\alpha\eta}{(ac)^2} = (1-r)e^{-\alpha}\sin(\eta). \tag{16}$$

We plot these relations in the complex plane with $c = c^*$ in Figure 3 for two values of $r > r^*$. Solutions of 15-16 correspond to intersections of the thin and thick lines in the plots. Please note that equations 15-16 are identical for the Ricker and logistic function, however, the value of c^* differs between the two. Since the differences are minor, we only plot the case of the Ricker function.

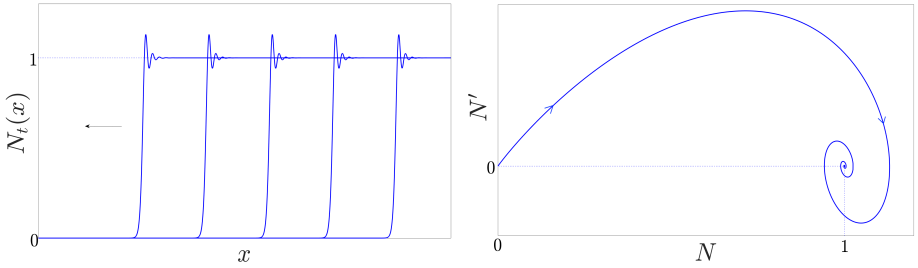

FIGURE 4. Solution of the integrodifference equation (left) and its phase plane (right), where F is the Ricker function with $r = 1.8$ and K is the Laplace kernel with $a = 15$.

We observe (i) that there are no real, negative eigenvalues since we chose $r > r^*$; and (ii) that the intersection points with negative real part move to the right as r increases. Hence, we expect to see a trajectory that spirals towards $(1, 0)$ in the delay equation system, and correspondingly a non-monotone traveling wave in the IDE when r is in some appropriate interval. We illustrate both of these objects in Figure 4.

Since the intersection points with negative real part move to the right as r increases, we expect to see eigenvalues with zero (and even positive) real part for large enough values of r. We calculate the smallest value of r, for which there is a complex eigenvalue with zero real part when $c = c^*$. We substitute $\alpha = 0$ in equations 15 and 16 and find

$$1 + \frac{\eta^2}{(ac^*)^2} = (r-1)\cos\eta, \tag{17}$$

$$(r-1)\sin\eta = 0. \tag{18}$$

From equation 18, it follows that $\eta = k\pi$, $k \in \mathbb{Z}$. The value of $\eta = \pi$ corresponds to the rightmost pair of complex eigenvalues with zero real part. Replacing this value of η into equation 17, we get

$$r = 2 + \frac{\pi^2}{(ac^*)^2}. \tag{19}$$

Since c^* is increasing in r, the right-hand side of this relation is decreasing while the left-hand side is increasing. Hence, there is a unique value r^{**} below which all eigenvalues with non-zero imaginary parts have negative real part. Again, as in the previous remark, we notice that the expression in 19 is independent of parameter a.

Since the equation is implicit we can solve it only numerically. We find $r^{**} = 2.5072$ for the Ricker function, and at $r^{**} = 3.1124$ for the logistic function. We note that for the Ricker function, $r^{**} < 2.526$, i.e., the threshold is still within the range where the two-cycle of the non-spatial map is stable (see Table 1). However, for the logistic function, we have $r^{**} > 2.449$, so that the threshold falls into the region where the two-cycle is unstable. (In fact, the non-spatial dynamics for the logistic equation are chaotic when $r = r^{**}$.) Thus, the necessary conditions for damped oscillations around $N = 1$ in the solution of the integrodifference equation, are satisfied when $1.0327 < r < 2.5072$ for the Ricker function, and $1.0686 < r < 2.449$ for the logistic function.

Figure 3 suggests that there are infinitely many eigenvalues with negative real part. This behavior would be typical for a delay system [11]. For that reason, we cannot exclude the existence of a non-monotone traveling-wave profile when $r > r^{**}$. However, simulations indicate that a Hopf bifurcation could occur in the delay system at $r = r^{**}$ and that the corresponding solution in the IDE is a traveling wave-train. We return to this phenomenon in Section 3.

2.3. **Existence of an Unstable Direction at** $(1, 0)$**.** For dynamical stabilization, we need to have a second traveling profile that starts at $(1, 0)$ and that moves slower than the first. In the simulations in Figure 1, we see such a profile connecting $N^* = 1$ and $N^* = n_+$ for the second-iterate operator $Q \circ Q$. Hence, we want to find conditions for which the state $(1, 0)$ for the delay system 6 with $G = Q$ has a real positive eigenvalue, and we want to know the resulting minimal speed of the profile.

We set $G = Q$ in 6 and denote by C the speed of the profile in the second-iterate operator $Q \circ Q$. We obtain the system

$$\begin{aligned} N'(y) &= n(y), \\ n'(y) &= a^2 N(y) - a^2 F(Q[N](y - C)). \end{aligned} \tag{20}$$

The equilibrium points of this system are given by $(N^*, 0)$, where $N^* \in \{0, n_-, 1, n_+\}$ denotes a fixed point of $F \circ F$. We linearize system 20 around $(N^*, 0)$ by letting $N(y) = N^* + M(y)$ and compute its eigenvalues. The linearization for n is obtained as

$$\begin{aligned} n'(y) &= a^2(N^* + M(y)) - a^2 F\left(\int K(y - C - z) F(N^* + M(z)) dz\right) \\ &\approx a^2 N^* + a^2 M(y) - a^2 F\left(\int K(y - C - z)[F(N^*) + F'(N^*) M(z)] dz\right) \\ &= a^2 N^* + a^2 M(y) - a^2 F\left(F(N^*) + F'(N^*) \int K(y - C - z) M(z) dz\right) \\ &\approx a^2 N^* + a^2 M(y) - a^2\left(F(F(N^*)) + F'(F(N^*)) F'(N^*) \int K(y - C - z) M(z) dz\right) \\ &= a^2 M(y) - a^2 (F \circ F)'(N^*) \int K(y - C - z) M(z) dz. \end{aligned}$$

Thus, the linearized system is

$$\begin{aligned} M'(y) &= n(y), \\ n'(y) &= a^2 M(y) - a^2 (F \circ F)'(N^*) \int K(y - C - z) M(z) dz. \end{aligned} \tag{21}$$

An exponential solution $[M(y), n(y)]^T = [k_1, k_2]^T e^{\lambda y}$ of 21 must satisfy the relations

$$\lambda k_1 e^{\lambda y} = k_2 e^{\lambda y} \tag{22}$$

and

$$\lambda k_2 e^{\lambda y} = a^2 k_1 e^{\lambda y} - a^2 k_1 (F \circ F)'(N^*) \int K(y - C - z) e^{\lambda z} dz. \tag{23}$$

We use a change of variables to compute the integral term as

$$\int K(y - C - z) e^{\lambda z} dz = \int K(z) e^{\lambda(y - C - z)} dz = e^{\lambda(y - C)} \frac{a^2}{a^2 - \lambda^2}, \tag{24}$$

provided that $-a < \lambda < a$. Substituting $\lambda k_1 = k_2$ from 22, we obtain

$$\lambda^2 = a^2 - (F \circ F)'(N^*)e^{-\lambda C}\frac{a^4}{a^2 - \lambda^2}.$$

Rearrangement leads to the transcendental problem

$$\left(\frac{a^2 - \lambda^2}{a^2}\right)^2 = (F \circ F)'(N^*)e^{-\lambda C}. \tag{25}$$

For explicit calculations, we substitute $N^* = 1$, so that $(F \circ F)'(1) = [F'(1)]^2 = (1 - r)^2 > 1$ for both, the Ricker and the logistic functions. In this case, 25 will not have solutions for $\lambda < 0$. For $0 < \lambda < a$, there can be up to two positive real roots. For exactly one root, we can derive a tangency condition by differentiating both sides of 25. The expressions simplify if we take square roots first. We obtain

$$\frac{4\lambda}{a^4} = C(1 - r)e^{-\lambda C/2}. \tag{26}$$

As before, we can combine 25 and 26 to obtain the following parametric representation for λ:

$$C = \frac{4\lambda}{a^2 - \lambda^2}, \qquad (1 - r) = \left(\frac{a^2 - \lambda^2}{a^2}\right)e^{\lambda C/2}. \tag{27}$$

This parametrization is exactly the same as the minimal 'generalized spreading speed' of the operator $Q \circ Q$, as defined in [2] and denoted by $c^*_{[1,n_+]}$, from the state $N^* = 1$ in the IDE 1.

Overall, we conclude that equation 25 has one real positive root for $C = c^*_{[1,n_+]}$ and two for $C > c^*_{[1,n_+]}$. Hence, a non-oscillating trajectory moving away from $(1, 0)$ may exist in the delay system 21 for all $C > c^*_{[1,n_+]}$ and $r > 2$. Correspondingly, a traveling profile that increases from the unstable state $N^* = 1$ may exist in the second-iterate IDE defined by the operator $Q \circ Q$. We summarize these results and illustrate how they relate to dynamical stabilization in the next section.

3. **Predictions and conditions for Dynamical Stabilization.** We list the results from the previous section in Table 2. For values $r < r^*$ we expect to see monotone traveling waves increasing from 0 to 1. As r increases, oscillations arise near the positive fixed point of the delay system so that non-monotone waves connecting 0 to 1 may exist for $r^* < r < r^{**}$ with $r^{**} > 2$. In both cases, the speed of the traveling waves is c^* as given by 5.

Shape of the traveling profile	Ricker function	Logistic function
Monotone on $[0, 1]$	$0 < r < 1.0327$	$0 < r < 1.0686$
Damped oscillations at $N = 1$	$1.0327 < r < 2.5072$	$1.0686 < r < 2.570$
Wavetrain around $N = 1$	$2.5072 < r < 2.692$	NA

TABLE 2. Shape of the traveling profile emerging from $N^* = 0$ in IDE 1 as a function of parameter r for the Ricker and the logistic function and with Laplace dispersal kernel. When the kernel has compact support, monotone traveling waves may not exist even if they do with a Laplace kernel [29].

At the same time, when $r > 2$ and $C > c^*_{[1,n_+]}$, there is an unstable direction in the second-iterate operator at $N^* = 1$ so that a traveling profile connecting 1 to $n_\pm$

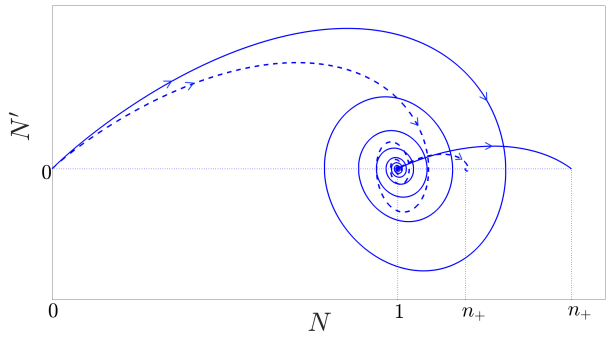

FIGURE 5. Phase plane of the solution in Figure 1. The solid curve corresponds to the Ricker function, the dashed curve to the logistic function, both with parameter $r = 2.2$. K is the Laplace kernel with $a = 15$.

may exist. This profile for the second-iterate operator corresponds to a temporally periodically alternating profile for the operator Q (Figure 1). If the profile for $Q \circ Q$ travels at speed C then the corresponding profile for Q travels at speed $C/2$. Hence, we expect to see dynamical stabilization when $c^* > C/2$ or $2c^* > C$. In [2], we showed that $2c^* > c^*_{[1,n_+]}$ in all the cases considered here. Hence, the necessary conditions for dynamical stabilization are satisfied when r is greater than 2 and less than the minimum of r^{**} and the upper limit of stability of the two-cycle of the non-spatial map. Whether and when dynamical stabilization actually occurs depends on the growth function.

For the Ricker function, the two-cycle loses stability when $r > 2.526 > 2.507 = r^{**}$, see Table 1. Numerically, we find dynamical stabilization for the entire range $2 < r < r^{**}$, as illustrated in Figure 5. At $r = r^{**}$, a pair of eigenvalues of the delay system 8 crosses the imaginary axis so that a Hopf bifurcation could occur. In that case, we could observe a periodic orbit in the 'phase plane' near $(1, 0)$. Such a periodic orbit would correspond to a traveling wave-train in the IDE. Indeed, in simulations, we observe a traveling profile that connects 0 to a traveling wave-train of oscillations, which correspond to a periodic orbit in the phase plane, see Figure 6. However, we recall that the delay system of the second-iterate operator always has a positive eigenvalue at $(1, 0)$, which allows for a traveling profile from 1 to $n_\pm$ in the IDE. We see that this profile eventually takes over and replaces the traveling wave-train (Figure 6). Whether this replacement always happens and how remains an open question outside the scope of our investigation here.

For the logistic function, the situation is similar for small r but different for larger values. We observe dynamical stabilization for $2 < r < 2.449$. The numerical simulations reveal a picture that is essentially identical to those for the Ricker function (plot not shown). For $r > 2.449$, the two-cycle of the non-spatial model becomes unstable and a stable four-cycle arises (Table 1). Accordingly, one can study the fourth-iterate of Q and the stability of its 8 fixed points in the 'phase plane'. From the point of view of spreading speeds, this analysis was carried out in [1] (e.g. Theorem 5.2.1). Extending the 'phase plane' theory presented here to this case seems less promising. Already for the second-iterate operator, we had to make certain approximations of the integral to arrive at the 'phase-plane' system

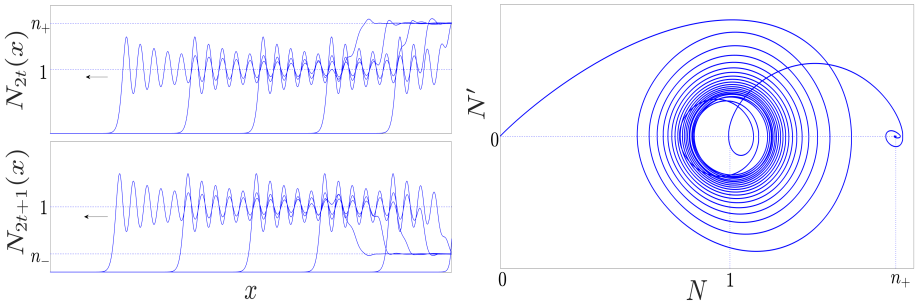

FIGURE 6. Solution of the integrodifference equation (left) and its phase plane (right), where F is the Ricker function with $r = 2.525$ and K is the Laplace kernel with $a = 15$.

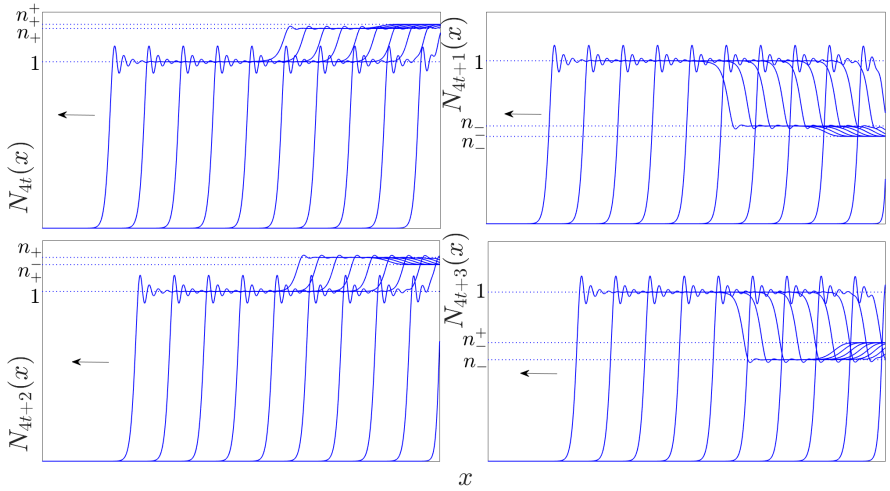

FIGURE 7. Solution of the integrodifference equation (left) and its phase plane (right), where F is the logistic function with $r = 2.5$ and K is the Laplace kernel with $a = 15$.

21. We speculate that the repeated approximation required for the fourth iterate could make the results too coarse to be useful.

Our numerical results for the logistic function, however, show that dynamical stabilization occurs at multiple levels in the following sense (see Figure 7). An initial traveling profile connects 0 to 1 and moves at high speed. It approaches the state at 1 in an oscillatory manner, but the state seems stable at first. Then a second profile moves in at a slower speed. This profile oscillates between the two states of the two-cycle, $n_\pm$. Again, these states are approached in an oscillatory manner, but they seem stable initially. Finally, an even slower oscillatory profile moves in that switches periodically between the four points on the non-spatial four-cycle of the system.

4. **Discussion.** Dynamical stabilization is a phenomenon by which an unstable state in a non-spatial model for population dynamics appears to be a stable state in the corresponding spatial model, at least for some time [30]. To be more precise,

the appearance of stability results from subsequent traveling profiles with different speeds. The transient state that emerges between two profiles increases in length if the first profile travels faster than the second. As the spatial extent of the transient state grows, so does the appearance of stability. This phenomenon has previously been observed and studied in systems of continuous-time reaction-diffusion equations [4, 22, 23, 31, 34], but not in the context of discrete-time integrodifference equations (IDEs). The advantage of studying IDEs in this context is that their scalar dynamics are not necessarily monotone (as they are for reaction-diffusion equations) so that the phenomenon can be observed in simpler models than for reaction-diffusion equations.

The instability that our non-spatial model displayed resulted from a flip bifurcation (which does not occur in time-continuous models). Consequently, dynamical stabilization for the operator Q is equivalent to the existence of stacked fronts for the operator $Q \circ Q$ [2]. The theory of stacked waves is well developed for reaction-diffusion equations [9, 14, 32], whereas it is only in its infancy for IDEs [24]. It is typically not connected to dynamical stabilization even though the phenomenon on an abstract level (see above) is the same.

Our analysis relied heavily on the use of the Laplace kernel 4, which allowed us to reduce the traveling-wave equation to a second-order delay differential equation. In the absence of this reduction, an analytical approach does not seem feasible. We explored the phenomenon of dynamical stabilization with a Gaussian dispersal kernel numerically. Overall, dynamical stabilization for the operator Q and stacked fronts for the operator $Q \circ Q$ can still be observed, although the details differ somewhat. For example, when using a Gaussian dispersal kernel with the same variance as the Laplace kernel, we may see non-monotone fronts instead of the monotone fronts in Figure 2 when $r = 1.03$ in the Ricker function, and we may also see damped oscillations behind the initial front with the Gaussian kernel where we see sustained oscillations with the Laplace kernel in Figure 6, please see Section 5.3 in [1] for illustrations and more details.

Another interesting observation is the difference in dynamical behavior between the Ricker and the logistic growth function. Whereas the latter shows dynamical stabilization even in the parameter range where a four-cycle occurs, dynamical stabilization breaks down in the former much earlier and undamped oscillations arise (Figure 6). For many practical purposes, the Ricker and logistic growth functions are often seen as equivalent with the Ricker function being more realistic (since it is positive everywhere) and the logistic function analytically more tractable (since it is a simple quadratic polynomial). Here, however, we observe a fundamental difference between the two. This difference remains for higher values of r, as we illustrate in Figure 8. When the non-spatial Ricker dynamics have a stable four-cycle, we observe the emergence of a traveling wave-train that is eventually replaced by a four-cycle. This is in stark contrast to the case of the logistic function, where we saw two instances of dynamical stabilization (Figure 7).

The periodic wave-trains that we observed in Figures 6 and 8 arise only in the spatial model, seemingly through a Hopf bifurcation in the 'phase plane' of the traveling profile. In our simulations, the wave-trains are eventually replaced by a two- or four-cycle. Indefinite traveling wave-trains in an IDE model for predator and prey species were first observed numerically in [16] and again in a parameterized model for blow-fly invasion [3]. Traveling wave-trains were observed in reaction-diffusion equations with predator-prey dynamics and studied in detail via so-called

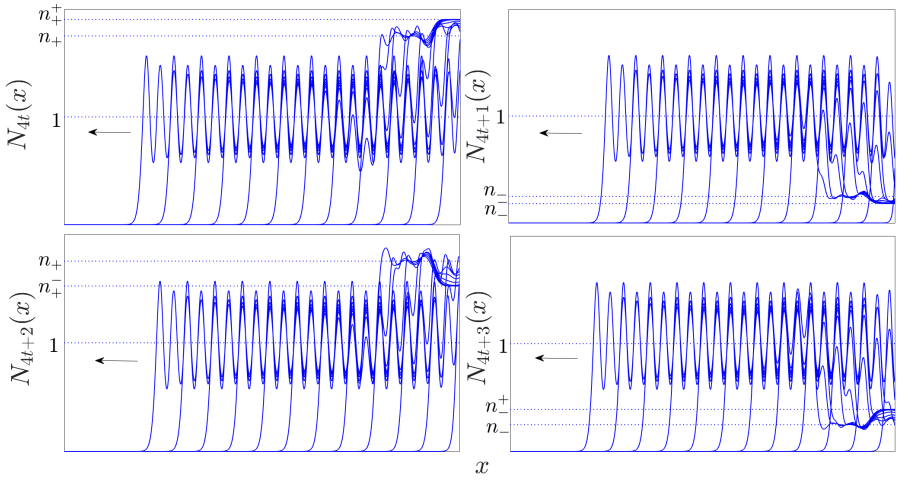

FIGURE 8. Solution of the IDE, with Ricker function and Laplace kernel ($a = 15$). The growth parameter is $r = 2.6$, so that the two-cycle $n_\pm$ is unstable for the Ricker dynamics and a stable four-cycle exist (denoted by $n_-^-, n_+^-, n_-^+, n_+^+$). Initial conditions are $N_0 = n_+^+ \chi_{[x\geq 10]}$.

λ-ω systems by [12, 15] (and many authors since, see [4, 34]), and also in integrodifferential equations [33]. The study of traveling wave-trains in IDEs is only in its infancy. Future research shall explore whether and under what conditions dynamical stabilization in IDEs with oscillatory dynamics arises and which of the techniques developed for reaction-diffusion equations will carry over to IDEs.

REFERENCES

[1] A. Bourgeois, *Spreading Speeds and Travelling Waves in Intergrodifference Equations with Overcompensatory Dynamics*, Master's thesis, University of Ottawa, https://www.ruor.uottawa.ca/handle/10393/34578, 2016.

[2] A. Bourgeois, V. LeBlanc and F. Lutscher, Spreading phenomena in integrodifference equations with non-monotone growth functions, *SIAM Journal of Applied Mathematics*, **78** (2018), 2950–2972.

[3] R. Coutinho, W. Godoy and R. Kraenkel, Integrodifference model for blowfly invasion, *Theoretical Ecology*, **5** (2012), 363–371.

[4] A. Dagbovie and J. Sherratt, Absolute stability and dynamical stabilisation in predator-prey systems, *Journal of Mathematical Biology*, **68** (2014), 1403–1421.

[5] G. de Vries, T. Hillen, M. Lewis, J. Müller and B. Schönfisch, *A Course in Mathematical Biology: Quantitative Modeling with Mathematical and Computational Methods*, Monographs on Mathematical Modeling and Computation, Society for Industrial and Applied Mathematics, 2006.

[6] R. Driver, *Ordinary and Delay Differential Equations*, Springer Science and Business Media, 2012.

[7] A. Ducrot, Spatial propagation for a two component reaction-diffusion system arising in population dynamics, *Journal of Differential Equations*, **260** (2016), 8316–8357.

[8] W. Fagan and J. Bishop, Trophic interactions during primary succession: Herbivores slow a plant reinvasion at mount st. helens, *The American Naturalist*, **155** (2000), 238–251.

[9] P. Fife and J. McLeod, The approach of solutions of nonlinear diffusion equations to travelling front solutions, *Archive for Rational Mechanics and Analysis*, **65** (1977), 335–361.

[10] A. Gharouni, M. Barbeau, A. Locke, L. Wang and J. Watmough, Sensitivity of invasion speed to dispersal and demography: an application of spreading speed theory to the green

crab invasion on the northwest atlantic coast, *Marine Ecology Progress Series*, **541** (2015), 135–150.
[11] J. Hale and S. Verduyn Lunel, *Introduction to Functional Differential Equations*, Applied Mathematical Sciences, Springer, New York, 1993.
[12] L. Howard and N. Kopell, Slowly varying waves and shock structures in reaction-diffusion equations, *Studies in Applied Mathematics*, **56** (1977), 95–145.
[13] S. Hsu and X.-Q. Zhao, Spreading speeds and traveling waves for nonmonotone integrodifference equations, *SIAM Journal on Mathematical Analysis*, **40** (2008), 776–789.
[14] M. Iida, R. Lui and H. Ninomiya, Stacked fronts for cooperative systems with equal diffusion coefficients, *SIAM Journal on Mathematical Analysis*, **43** (2011), 1369–1389.
[15] N. Kopell and L. Howard, Plane wave solutions to reaction-diffusion equations, *Studies in Applied Mathematics*, **42** (1973), 291–328.
[16] M. Kot, Discrete-time traveling waves: Ecological examples, *Journal of Mathematical Biology*, **30** (1992), 413–436.
[17] M. Kot, M. Lewis and P. van den Driessche, Dispersal Data and the Spread of Invading Organisms, *Ecology*, **77** (1996), 2027–2042.
[18] M. Kot and W. Schaffer, Discrete-time growth-dispersal models, *Mathematical Biosciences*, **80** (1986), 109–136.
[19] M. Lewis, S. Petrovskii and J. Potts, *Mathematics behind biological invasions*, Interdisciplinary Applied Mathematics, Springer, 2016.
[20] B. Li, M. Lewis and H. Weinberger, Existence of traveling waves for integral recursions with nonmonotone growth functions, *Journal of Mathematical Biology*, **58** (2009), 323–338.
[21] G. Lin, Traveling wave solutions for integro-difference systems, *Journal of Differential Equations*, **258** (2015), 2908–2940.
[22] H. Malchow and S. Petrovskii, Dynamical stabilization of an unstable equilibrium in chemical and biological systems, *Mathematical and Computer Modelling*, **36** (2002), 307–319.
[23] H. Malchow, S. Petrovskii and E. Venturino, *Spatiotemporal Patterns in Ecology and Epidemiology*, Chapman and Hall CRC, 2008.
[24] N. Marculis and R. Lui, Modelling the biological invasion of Carcinus maenas (the European green crab), *Journal of Biological Dynamics*, **10** (2016), 140–163.
[25] R. May, Biological populations obeying difference equations: Stable points, stable cycles, and chaos, *Journal of Theoretical Biology*, **51** (1975), 511–524.
[26] M. Neubert, M. Kot and M. Lewis, Dispersal and pattern formation in a discrete-time predator-prey model, *Theoretical Population Biology*, **48** (1995), 7–43.
[27] M. Owen and M. Lewis, How predation can slow, stop or reverse a prey invasion, *Bulletin of Mathematical Biology*, **63** (2001), 665–684.
[28] S. Pan, Invasion speed of a predator-prey system, *Applied Mathematics Letters*, **74** (2017), 46–51.
[29] S. Pan and G. Lin, Propagation of second order integrodifference equations with local monotonicity, *Nonlinear Analysis Real World Applications*, **12** (2011), 535–544.
[30] S. Petrovskii and H. Malchow, A minimal model of pattern formation in a prey-predator system, *Mathematical and Computer Modelling*, **29** (1999), 49–63.
[31] S. Petrovskii and H. Malchow, Critical phenomena in plankton communities: KISS model revisited, *Nonlinear Analysis: Real World Applications*, **1** (2000), 37–51.
[32] J. Roquejoffre, D. Terman and V. Volpert, Global stability of traveling fronts and convergence towards stacked families of waves in monotone parabolic systems, *SIAM Journal on Mathematical Analysis*, **27** (1996), 1261–1269.
[33] J. Sherratt, Invasion generates periodic traveling waves (wavetrains) in predator-prey models with nonlocal dispersal, *SIAM Journal on Applied Mathematics*, **76** (2016), 291–313.
[34] J. Sherratt, A. Dagbovie and F. Hilker, A mathematical biologist's guide to convective and absolute stability, *Bulletin of Mathematical Biology*, **76** (2014), 1–26.
[35] H. Weinberger, Asymptotic behavior of a model in population genetics, *Nonlinear partial differential equations and applications*, **648** (1978), 47–96.
[36] H. Weinberger, Long-time behavior of a class of biological models, *SIAM Journal on Mathematical Analysis*, **13** (1982), 353–396.
[37] H. Weinberger and X.-Q. Zhao, An extension of the formula for spreading speeds, *Mathematical Biosciences and Engineering*, **7** (2010), 187–194.
[38] T. Yi and X. Zou, Asymptotic behavior, spreading speeds and traveling waves of nonmonotone dynamical systems, *SIAM Journal on Mathematical Analysis*, **47** (2015), 3005–3034.

[39] Z.-X. Yu and R. Yuan, Properties of traveling waves for integrodifference equation with non-monotone growth functions, *Zeitschrift fuer Angewandte Mathematik und Physik*, **63** (2012), 249–259.

E-mail address: abour115@uottawa.ca
E-mail address: vleblanc@uottawa.ca
E-mail address: flutsche@uottawa.ca